Metallurgical and Materials Data 2, no. 1 (2024): 29-33

Publisher: Association of Metallurgical Engineers of Serbia

Metallurgical and Materials Data

www.metall-mater-data.com

Nucleation of topologically equivalent phases after annihilation of topological defects

Milan Svetec*

[1]Pomurje Science and Innovation Centre, Lendavska ulica 28, Rakičan, 9000 Murska Sobota
[2]University of Maribor, Faculty of natural sciences and mathematics, Koroška c. 160, 2000 Maribor

ARTICLE INFORMATION:

https://doi.org/10.56801/MMD22

Received: 23 February 2024
Accepted: 2 April 2024

Type of paper: Research paper

ABSTRACT

The annihilation of radial and hyperbolic point defects within an infinite cylinder of radius R in nematic liquid crystals using Brownian molecular dynamics simulations is studied. Unlike some other studies, where they focus on individual phases of annihilation, this paper considers the entire course of annihilation, both before and after the collision of the two defects. After the collision, merging of defects, and building of a ring disclination structure, the system can experience a structural transition into another topologically equivalent nematic structure, triggered by the nucleation of the ring disclination structure. In the article, the condition under which the transition to the topologically equivalent final structure of the molecular arrangement occurs is quantitatively determined. In addition, a comparison of the temporal evolution of the final stable structure is discussed, where, based on a simple dissipation relation, we obtain an equation that agrees well with the simulation results.

Keywords: topological defects, annihilation of defects, nucleation, liquid crystals, Brownian molecular dynamics.

1. Introduction

Topological defects are very important structures in the fields of solid (and soft) matter physics and materials science. Research is carried out in various areas (Skogvoll et al.,2023) from Bose-Einstein condensates, via liquid crystals to solid crystals and metal alloys (Skogvoll et al., 2023, Cheng et al.,2024, Gao et al., 2019). Even more, topological defects are a frequent subject of study in the fields of particle physics and even cosmology and string theory (Fumeron and Berche, 2023). In short, topological defects are universally present in practically the entire field of physics and the study of materials. Even the 2016 Nobel Prize in Physics was awarded to theoretical physicists whose work established the role of topology in understanding exotic forms of matter. In this paper, the focus is on the annihilation of topological defects in liquid crystals through Brownian molecular dynamics simulations. Liquid crystals are an effective tool for studying many phenomena, as they are easily accessible (their study is not associated with high costs) and responsive to various influences (temperature, density, external electric, and magnetic fields, etc.) (de Gennes et al.,1993). In this study, the focus is on liquid crystals in the so-called nematic phase. The liquid crystals are considered as elongated molecules, where the elongated axis in the average of several molecules is denoted by the unit vector $\vec{l}$. Here $\vec{l} \in \mathbb{S}^2$ and $\mathbb{S}^2 := \{\vec{p} \in \mathbb{R}^3 : |\vec{p}| = 1\}$ is the unit sphere. The liquid crystal molecules are non-polar; therefore $\vec{l}$ and $-\vec{l}$ have the same meaning. Let f be the probability density of the molecular orientations through the liquid crystal sample. In the isotropic phase the orientations (as well as centers of mass) are randomly distributed over all directions. Therefore, in the isotropic hase, f is a constant. In the nematic phase, however, there is a preferred direction (anisotropy), designated by a unit vector $\vec{n}$, called director (field), where at the mesoscopic scale after averaging the preferential direction emerges. Defects are usually described as small regions where the local director field $\vec{n}(\vec{r})$ exhibits discontinuous change in orientation. Therefore, in that region, the director field cannot be uniquely defined (de Gennes et al.,1993). Such a singular region is isotropic, while a nonsingular region can be described as uniaxial in the nematic phase (de Gennes et al.,1993). In the nematic phase $f = f(\vec{l})$ is not constant and we can define a second-order tensor as (Virga, 1994)

$$\underline{M} := \int_{\mathbb{S}^2} \vec{l} \otimes \vec{l} f(\vec{l}) da \qquad 1$$

Here $\otimes$ denotes the tensorial product of two vectors, and a is the area measure on $\mathbb{S}^2$. There can be shown (Virga, 1994) that $Tr(\underline{M}) = 1$, where Tr denotes the trace of a tensor, and $\underline{M}^T = \underline{M}$ which tells us that

* Corresponding author.
E-mail address: milan.svetec@zis.si (Milan Svetec).

$\underline{M}$ is symmetric. In the isotropic phase, where f is a constant, we get (Virga, 1994) $\underline{M} = \underline{M_0} = \frac{1}{3}\underline{I}$, where $\underline{I}$ denotes the unit tensor. To properly describe a phase transition, we have to define the order parameter. Order parameter must be some quantity which disappears in the phase not interesting to us (here this would be the isotropic phase) and have nonzero value in the other (in our case - nematic) phase. In the case of nematic liquid crystals (LC) the order parameter must be second-order tensor (de Gennes et al.,1993). Therefore, we define $\underline{Q} := \underline{M} - \underline{M_0}$ as order parameter. The order parameter $\underline{Q}$ is a traceless and symmetric tensor and can in his eigenframe be represented as $\underline{Q} = \sum_{i=1}^{3} \lambda_i \hat{e}_i \otimes \hat{e}_i$, where λ_i are the eigenvalues and $\hat{e}_i$ are the eigenvectors of the order parameter. Because $\underline{Q}$ is traceless, there are only two independent eigenvalues e.g. $\lambda_3 = -(\lambda_1 + \lambda_2)$. Tensorial order parameter $\underline{Q}(\vec{r})$ is continuous everywhere including the core of a defect (de Gennes et al.,1993). In contrast to $\vec{n}(\vec{r})$ it can smoothly describe changes between the isotropic, uniaxial, and biaxial nematic states. If as in our case the molecules of LC are considered as elongated molecules or "sticks", there is only one independent eigenvalue. This is then so-called uniaxial approximation of the system. For uniaxial system we can write the order parameter tensor as (Virga, 1994)

$$\underline{Q} = s\left(\vec{n} \otimes \vec{n} - \frac{1}{3}\underline{I}\right) \qquad 2$$

Here $\vec{n} = \hat{e}_3$ and $s = -\lambda_1$. For the uniaxial case we can write also $s = \frac{3}{2}\left\langle cos^2\vartheta - \frac{1}{3}\right\rangle$ (Virga, 1994), where ϑ is the angle between $\vec{l}$ and $\vec{n}$.

The brackets $\langle ... \rangle$ represent average over the mesoscopic scale where $\vec{n}$ is defined.

Among widely used geometries, nematics in cylindrical capillaries exhibit a particularly rich diversity of structures. They primarily depend on molecular orientation at the walls of the confining capillary. The imposed orientation (anchoring) of the molecules at the lateral wall can be arbitrary, but in most cases, it is homeotropic. Here, the long axes of the molecules are oriented perpendicularly to the lateral wall. In cylindrical cavities with homeotropic anchoring, there are basically four different types of structures (Bradač et al.,1998). Two of them are depicted in Figure 1. On the Figure 1 (a) there is an escaped radial (ER) structure, where molecules approaching the cylindrical axis gradually "escape" from radial towards the axial direction, and (b) planar polar with two line defects (PPLD), where molecules are constrained to the azimuthal plane and the two line defects are parallel to the major cylinder axis. Those two structures are the only possible equilibrium end structures in the simulations, and they are topologically equal. The stability of the named structures is mostly influenced by an intermolecular potential, the size of the capillary, and the elastic properties of the confined LC system.

On Figure 1 we can see the planar configurations of the director field $\vec{n}(\vec{r})$. Here we can write $\vec{n} = \cos\psi\hat{e}_1 + \sin\psi\hat{e}_2$. Suppose that $\vec{n}$ is continuous everywhere in the plane except at the points where defects are expected. Say that one of such points is *P* and the director field is continuous everywhere at least at the distance *d* from *P*. We consider then circle centered at *P* with the radius *d*. Let us traverse the circle in a counterclockwise way and count counterclockwise increments in angle ψ as positive, and clockwise increments, as negative. Since $\vec{n}$ is continuous on the circle the following contour integral must be multiple of 2π (Skogvoll et al., 2023)

$$q = \frac{1}{2\pi}\oint_{\partial\mathcal{M}} d\psi \qquad 3$$

where q is the so-called topological charge (or winding number) and $\partial\mathcal{M}$ is a closed circuit in real space around *P*. Because of the Z_2 symmetry the value of q is restricted to positive/negative integers or half-integers (Fumeron et al., 2023). The half-integer values are valid because of the head to tail invariance of the vectors $\vec{l}$. Free energy of the system is proportional to q^2, therefore the half-integer winding numbers are preferred by the system and only distortions with the lowest winding number are observed (Fumeron et al., 2023).

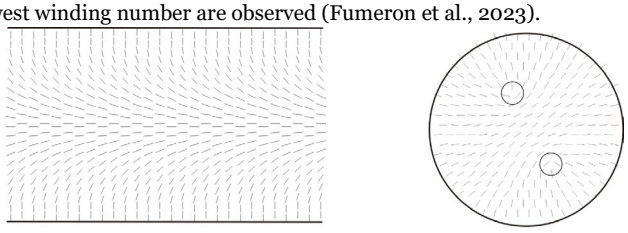

(a) (b)

Fig. 1. (a) The escaped radial (ER) end-configuration of the annihilation of radial and hyperbolic point defects. We see here the *x*-*z* plane cross-section of the capillary with horizontal *z* axis. (b) The planar polar end-configuration with two line defects (PPLD) where we see the *x*-*y* plane cross-section of the capillary. The line defects run along the long (*z*) axis, therefore on this cross-section we only can see (encircled with two small circles) the defects with the winding number +1/2.

In this paper, the focus is on the annihilation of two topological defects with opposite winding numbers (+1 and -1) where the defect with winding number +1 is sometimes called a radial defect (or hedgehog), and the defect with winding number -1 we often call the hyperbolic defect (or anti-hedgehog). Both defects are enclosed within the capillary of the radius *R* and length *L* with the homeotropic anchoring at the lateral walls. Here $R = N_R b$, and $L = N_Z b$, where N_R and N_Z are integers in radial and *z* axis directions, respectively, and *b* is some typical size in the system (lattice spacing). In reality the radius of the capillary is about 100 nm, therefore $b \cong 2$ nm.

Most studies of the annihilation of topological defects focus on the pre-collision phase, in this case, the whole process can be simulated, even after the collision.

Using a simple setup for the nucleation of a new phase, we calculate the critical value of the size of the joint defect after the collision of the two topological defects. This value gives us an approximation of the size of the so-called ring structures, so that the final topologically equivalent phase will develop. In the following, we also compare the spatial and temporal evolution of the final structure of the common annular defect after the collision. Using a simple dissipation relation, we obtain an equation that adequately approximates both the spatial and temporal evolution of the equilibrium final structure.

2. Modeling

In this study, the semi-microscopic approach is used. The dynamics of the system are studied with the Brownian orientational molecular dynamics enabling access to the macroscopic time scales. In this approach, the "molecules" interact via a generalized Van der Waals pairwise interaction, which to some extent considers the elastic anisotropy of nematic LC. The interaction of the pair of rod-like LC "molecules" at $\vec{r}_i$ and $\vec{r}_j = \vec{r}_i + \Delta\vec{r}$, oriented along $\hat{e}_i(\vec{r}_i)$ and $\hat{e}_j(\vec{r}_j)$ is expressed as (Bradač et al., 2003)

$$V_{ij} = -\frac{J}{|\Delta\vec{r}|^6}\left(\hat{e}_i \cdot \hat{e}_j - \frac{3\varepsilon}{|\Delta\vec{r}|^2}\left(\hat{e}_i \cdot \Delta\vec{r}\right)\left(\hat{e}_j \cdot \Delta\vec{r}\right)\right)^2 \quad 4$$

Here J is the positive interaction constant and ε measures the degree of orientational anisotropy. For $\varepsilon = 0$ the isotropic Maier-Saupe (also called Lebwohl-Lasher) kind of interaction is obtained (Lebwohl et al., 1972). For $\varepsilon = 1$ the induced dipole – induced dipole interaction is established (Skačej et al., 1997). This model reasonably describes properties of nematic LCs for $\varepsilon < 0.3$. Note that the term molecule stands for a cluster of (real) molecules. Molecules are allowed to wander around the points of the 3D hexagonal lattice with spacing *b*. By such a box restricted dynamics the lattice induced ordering anisotropy is avoided known to appear in regular lattices. The local orientation of the *i*-th molecule in the laboratory frame is parametrized as $\hat{e}_i = \hat{e}_x \sin\Theta\cos\Phi + \hat{e}_y \sin\Theta\sin\Phi + \hat{e}_z \cos\Theta$, where angles $\Theta = \Theta(\vec{r}_i, t)$ and $\Phi = \Phi(\vec{r}_i, t)$ are the variational parameters.

The Brownian molecular dynamics method is used to follow the rotational dynamics of the system. At each time interval Δt (one sweep) the molecular orientation of the system is updated in the local frame using

$$\Psi^{(l)}(\vec{r}_i, t+\Delta t) = \Psi^{(l)}(\vec{r}_i, t) - \sum_{j\neq i}\frac{D_{ij}^{(l)}}{kT}\Delta t\frac{\partial V_{ij}}{\partial\Psi^{(l)}} + \Psi_{r,i}^{(l)} \quad 5$$

where $\Psi^{(l)}$ represents either Θ or Φ and the superscript (*l*) indicates the local molecular frame in which the rotation diffusion tensor $D_{ij}^{(l)}$ is diagonal. In calculations its eigenvalues are assumed to be degenerated and equal to *D*. The quantity *k* is the Boltzmann constant, *T* is the temperature, and $\Psi_{r,i}^{(l)}$ is the stochastic variable obeying the Gaussian distribution. The distribution is centered at $\Psi_{r,i}^{(l)} = 0$ and the width of the distribution is proportional to $\sqrt{T}$. The corresponding multiplicative constant is chosen to yield a correct equilibrium value of the nematic uniaxial order parameter. The summation in Eq. (5) is limited to neighbors within a sphere of a radius *2b*. The shortest time interval Δt of the model in the simulation is set by $\Delta t\, D = 0.01$. For a typical nematic LC this ranges within the interval $\Delta t \cong 0.001$ ms to $\Delta t \cong 0.1$ ms. depending on the size of a "molecule".

Following the Landau - de Gennes description of the system in nematic phase, we can use our tensorial order parameter $\underline{\underline{Q}}$ to write the free energy of the system in the following way (Fumeron et al., 2023)

$$F = \int\left[A(T)\,\mathrm{Tr}\left(\underline{\underline{Q}}^2\right) - B\,\mathrm{Tr}\left(\underline{\underline{Q}}^3\right) + C\,\mathrm{Tr}\left(\underline{\underline{Q}}^2\right)^2\right]d^3r + F_E + F_S \quad 6$$

Here $A(T) = A_0(T - T_*)$, where A_0 is positive material constant, as well as *B* and *C*, and T_* is nematic supercooling temperature. In (6) and F_S are elastic and surface free energies of the system, respectively. The elastic term in the above equation contains changes in the director field that are spatially dependent. This can be given by the gradient of the tensor order parameter, but a notation that emphasizes the three characteristic perturbations in the director field and is named after Frank-Oseen is commonly used (Fumeron et al., 2023)

$$F_E = \int\left[\frac{K_1}{2}|\nabla\cdot\vec{n}|^2 + \frac{K_2}{2}|\vec{n}\cdot(\nabla\times\vec{n})|^2 + \frac{K_3}{2}|\vec{n}\times(\nabla\times\vec{n})|^2\right]d^3r \quad 7$$

where K_1, K_2 and K_3 are splay, twist and bend elastic constants, respectively. This expression is commonly simplified into so called "one constant approximation" (Virga, 1994)

$$F_E = \int\left[\frac{K}{2}|\nabla\vec{n}|^2\right]d^3r \quad 8$$

Here is single elastic constant, and for 5CB liquid crystal its value has been measured as approximately 10^{-11} N. Surface term enters the system with the boundary conditions (anchoring). Usually, the surface term can be expressed as (Virga, 1994)

$$F_S = \int\left[\frac{w}{2}\mathrm{Tr}\left(\underline{\underline{Q}} - \underline{\underline{Q}}_S\right)^2\right]d^2r \quad 9$$

where *w* is positive anchoring constant and $\underline{\underline{Q}}_S$ describes the nematic ordering imposed by the confining substrate. In the strong anchoring limit $w \to \infty$ there is $\underline{\underline{Q}} = \underline{\underline{Q}}_S$. Therefore, because of strong anchoring conditions surface term is not important in the calculations.

3. Results and discussion

In the simulation, the values $2N_r$ and N_Z are typically chosen between 40 and 80. The cylinder axis is set along the z direction of the laboratory coordinate system. The lateral surface strongly enforces the neighboring molecules orientation along the surface normal, corresponding to the strong homeotropic anchoring. At a distance *L* along the cylinder axis, periodic boundary conditions are imposed simulating an infinite cylindrical capillary. The equilibrium nematic director configurations of the system are topologically equivalent escaped (ER) structure or planar structure with two line defects (PPLD) shown in Fig. 1. For radii above the critical value $R_C(\varepsilon)$ the ER structure is stable and the PPLD structure for $R < R_C(\varepsilon)$. The value of $R_C(\varepsilon)$ increases with ε. In our simulations (Bradač et al., 2003) $R_C(0) = 16\,b$ and $R_C(0.07) = 25\,b$. In the simulation initially the radial and the hyperbolic defect are placed on the cylinder axis. The initial separation of defects is close enough so that the interaction between defects is sufficiently strong. For such initial conditions, the collision of defects and further evolution into the final equilibrium structure are reached in a computationally accessible time. On the other hand, the separation is large enough so that the cores of defects reach their quasi-equilibrium configuration before being apparently influenced by each other.

The defects, which are in the beginning of the simulation separated by $\xi_d^{(0)}$ approaching their quasi-equilibrium configuration attain ring-like structure where ring is formed about the core of the defect as a closed line defect, which shows some biaxial structure (Svetec et al., 2006, De Luca et al., 2007). The ring structure of the both defects forms after several 1000 of steps in the simulation. The points belonging to the ring (red and blue ellipses in Figure 2) correspond to the largest connected local distortions in nematic ordering within the core of defect (Svetec et al., 2006). In the continuum Q-tensor representation by crossing the ring the exchange of $\underline{\underline{Q}}$ eigenvalues takes place. Therefore, in this case the core of defect exhibits locally roughly the cylindrical symmetry. Due to the confinement, after the creation the rings tend to orient with their symmetry axes perpendicularly to the cylinder axis, breaking the cylindrical symmetry of the structure. After a certain time, which depends on the coefficient ε, which represents the orientational anisotropy in the system, the two rings merge into one common ring structure.

The further course of the simulation depends on the size of the overall ring structure thus obtained. At a constant capillary size, there is a certain threshold value of the parameter ε_C, when for larger values of this parameter, the PPLD form is established as the final equilibrium structure in the capillary, and for values of ε that are smaller than ε_C, the final equilibrium structure is equal to ER. With the growing size of

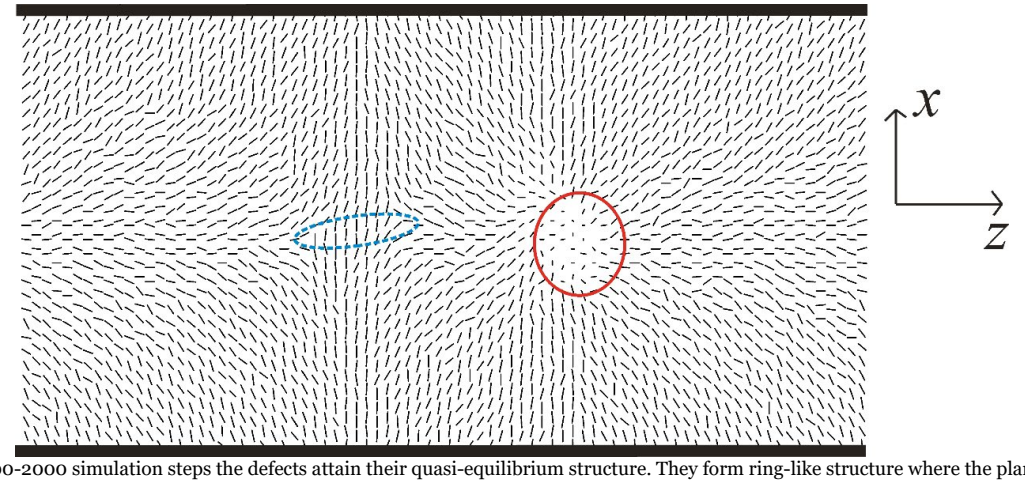

Fig. 2. After about 1000-2000 simulation steps the defects attain their quasi-equilibrium structure. They form ring-like structure where the plane in which the ring lies is rotating about the long (z) axis. The ring structure of the radial defect is depicted as a red ellipse where the molecules within the ring structure are directed along *y*-axis (on the figure we see only dots), while the ring structure of the hyperbolic defect in the figure depicted as dotted blue ellipse is almost perpendicular to the *x*-axis and the molecules within the ring structure are directed along the *x*-axis.

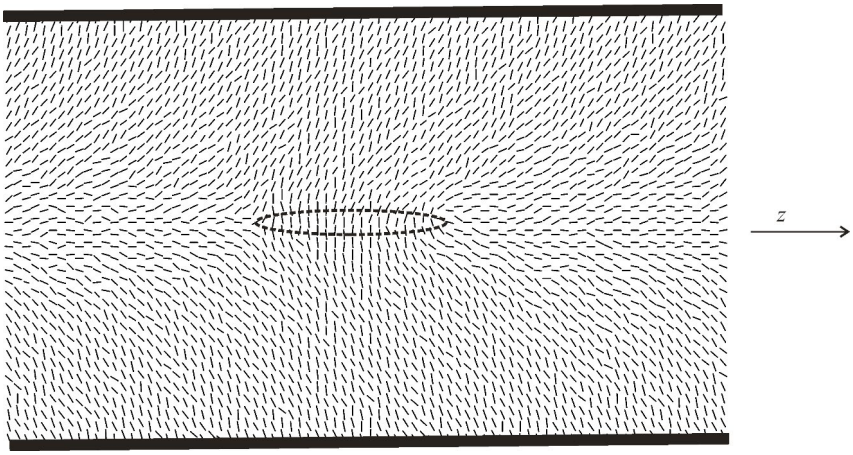

Fig. 3. After the collision of radial and hyperbolic defects, a common structure is formed, where both rings of both defects merge into one common ring structure and the molecules surrounded by this ring form the core (nucleus) of the new PPLD phase, which must be large enough (compared to the size of the system) to extend to the entire system. If the resulting nucleus is too small, the nucleus begins to shrink and finally disappears, and the final equilibrium ER structure is formed.

the capillary also the value of ε_C increases. In Figure 3, we can see in the *x*-*z* plane a common ring structure after the collision of defects, which have been marked with a dotted black ellipse. If the long axis is in the *z* direction, we see that in the core of the common structure, molecules are oriented along the *x* axis. Now if the size of that ring structure is big enough, the PPLD end equilibrium structure will be formed.

To the molecules inside the ring structure the free energy density f_P can be assigned and to the molecules outside the ring structure the free energy density f_E. In the following the ring structure together with the contained and mostly affected LC molecules is approximated as to be spherical nucleus. Thickness of the loop is neglected. The free energy of the system reads

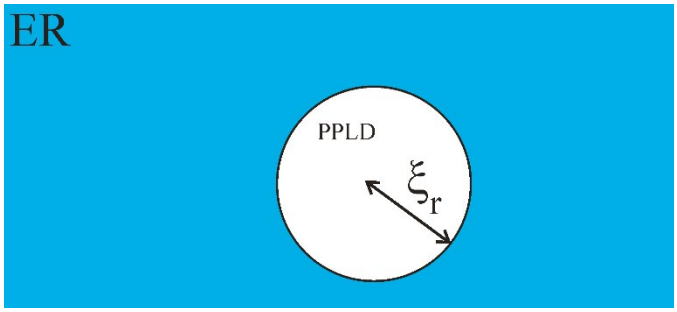

Fig 4. After the collision of defects, they merge into common ring structure with the inner PPLD-like structure. The ring structure is approximated by the sphere with the radius ξ_r. Free energy within the sphere is equal to f_P, the ER structure outside the sphere has the free energy f_E.

$$F = \frac{4\pi}{3} f_P \xi_r^3 + 4\pi \xi_r^2 \sigma + f_E \left(V - \frac{4\pi}{3} \xi_r^3 \right) \qquad 10$$

Here σ is the surface tension of the emerged ring structure, and V is the volume of the whole capillary. If you write $\Delta f = f_P - f_E$ and minimize (10) with respect to ξ_r, you get $\xi_r^{(C)} = -\frac{2\sigma}{\Delta f}$, where the $\Delta f < 0$ has to be considered. If you make another approximation $|\Delta f| \approx \frac{K}{R^2}$, where K is suitable elastic constant and R correlation length, you get

$$\xi_r^{(C)} = \frac{2R^2\sigma}{K} \qquad 11$$

For PPLD ring structure with $\xi_r > \xi_r^{(C)}$ the final equilibrium PPLD structure in the whole capillary will evolve. For PPLD ring structures, smaller than this, the ring structure will diminish and disappear, and the end ER structure will form.

In the following the time evolution and the dependence of the evolving PPLD end-structure on the degree of orientational anisotropy ε will be investigated. For that purpose we establish the following dimensionless quantities: $\tau = \frac{t}{t_C} - 1$ is the eigentime, where t_C is the so-called collision time, that is the time of collision for point defects in

different simulations; and $\mu = \frac{\xi_r}{R}$. For the annihilation of the closed line defects in the bulk there holds for the several systems $\xi_r \propto \tau^{1/2}$ (Pargellis et al., 1991), but in this case the results show more Lifshitz-Slezov kind of dynamics (Lifshitz et al., 1981), therefore you can write the following non-dimensional dissipation relation

$$\mu^2 \frac{\partial \mu}{\partial \tau} = D(\varepsilon)(\varepsilon - \varepsilon_C) \qquad 12$$

Here *D(ε)* is a non-dimensional dissipation function, which depends on the interaction potential, and ε_C is the "critical" value of the degree of orientational anisotropy, which separates the evolvement of the system into the ER or PPLD end-structure. The inner structure of the dissipation function will not be discussed here. Solving differential equation (12) you obtain

$$\mu(\varepsilon, \tau) = \sqrt[3]{\mu_0^3(\varepsilon) + D(\varepsilon)(\varepsilon - \varepsilon_C)\tau} \qquad 13$$

Here μ_0 represents the relative radius of the ring structure at $\tau = 0$. From the last equation you can infer that the ring structure in the case if $\varepsilon < \varepsilon_C$ would shrink in time and for the system where $\varepsilon > \varepsilon_C$ the ring structure would get larger.

In the Figure 5 there are results of the simulation compared with the model introduced by the dissipation relation in (12). On the Figure 5 (a) there are the sizes of the ring structure after the collision of the defects at $\tau = 0$ shown with the dots (in fact this is the graph of $\mu_0(\varepsilon)$). In the simulations the threshold value for the coefficient $\varepsilon_C = 0.07$ separating the ER and PPLD outcome of the simulation. On the Figure 5 (b) we have a temporal evolution of the ring structure after the collision. In the Figure 5 (b) we have two cases for ER end-structure and two cases for PPLD end-structure. For the ER structure the formed ring structure at $\tau = 0$ starts to decrease and eventually disappears, whereby on the other hand the ring structure evolving towards PPLD end-structure after the collision starts to grow.

4. Conclusion

In the paper, the numerical study of the annihilation of nematic point defects deep in the nematic phase is performed. The rod-like molecules, interacting via the generalized induced dipole-induced dipole potential are considered, whose elastic anisotropy is mainly characterized by a small positive dimensionless parameter ε. The time evolution of the system is governed via the Brownian molecular dynamics, which enables the access of macroscopic time scales. A local orientation of each molecule is determined by two angles, which represent the dynamic variational variables of the problem. Note that no symmetry constrains were imposed in simulations, where the number of molecules typically ranged between 10^4 and 10^6. Soon after the start of the simulation the defects form a ring-like structure, where the symmetry axis of the "rings" is perpendicular to the long axis of the capillary. In the course of time, the "rings" rotate about the long axis of the system. After the collision of defects, the size of emerged ring structure was followed dependent on the intermolecular potential, which was altered by different values of the orientational anisotropy coefficient ε. Increasing the orientational anisotropy coefficient, the size of emerging ring structure grows like $\varepsilon^{1/3}$. Further the dynamics of the ring disclination structure was investigated using simple dissipation relation. The temporal evolution of emerged structure was also followed by numerical simulations. Dynamics is crucially affected by the intermolecular potential. It was found that growth and alternatively decay are faster as the orientational anisotropy coefficient differs from ε_C.

References

Bradač, Zlatko, Samo Kralj, Milan Svetec, and Slobodan Žumer. "Annihilation of nematic point defects: postcollision scenarios." Physical Review E 67, no. 5 (2003): 050702.

Bradač, Zlatko, Samo Kralj, and Slobodan Žumer. "Molecular dynamics study of nematic structures confined to a cylindrical cavity." Physical Review E 58, no. 6 (1998): 7447.

Cheng, Yuan, Xinbao Zhao, Wanshun Xia, Quanzhao Yue, Yuefeng Gu, and Ze Zhang. "The overview of the formation mechanisms of topologically close-packed phases in Ni-based single crystal superalloys." Materials & Design (2023): 112582.

De Gennes, Pierre-Gilles, and Jacques Prost. The physics of liquid crystals. No. 83. Oxford university press, 1993.

De Luca, Gino, and Alejandro D. Rey. "Ringlike cores of cylindrically confined nematic point defects." The Journal of chemical physics 126, no. 9 (2007).

Fumeron, Sébastien, Bertrand Berche, and Fernando Moraes. "Geometric theory of topological defects: methodological developments and new trends." Liquid Crystals Reviews 9, no. 2 (2021): 85-110.

Fumeron, Sébastien, and Bertrand Berche. "Introduction to topological defects: from liquid crystals to particle physics." The European Physical Journal Special Topics 232, no. 11 (2023): 1813-1833.

Gao, Ningbo, S-G. Je, M-Y. Im, Jun Woo Choi, Masheng Yang, Qin-ci Li, T. Y. Wang et al. "Creation and annihilation of topological meron pairs in in-plane magnetized films." Nature communications 10, no. 1 (2019): 5603.

Lebwohl, Paul A., and Gordon Lasher. "Nematic-liquid-crystal order—a Monte Carlo calculation." Physical Review A 6, no. 1 (1972): 426.

Lifshitz E. M, Pitaevskii L. P. "Physical Kinetics" Vol. 10 of Landau and Lifshitz course of theoretical physics, Oxford: Pergamon Press, 1981.

Pargellis, Andrew, Neil Turok, and Bernard Yurke. "Monopole-antimonopole annihilation in a nematic liquid crystal." Physical review letters 67, no. 12 (1991): 1570.

Skačej, Gregor, V. M. Pergamenshchik, A. L. Alexe-Ionescu, Giovanni Barbero, and Slobodan Žumer. "Subsurface deformations in nematic liquid crystals: The hexagonal lattice approach." Physical Review E 56, no. 1 (1997): 571.

Skogvoll, Vidar, Jonas Rønning, Marco Salvalaglio, and Luiza Angheluta. "A unified field theory of topological defects and non-linear local excitations." npj Computational Materials 9, no. 1 (2023): 122.

Svetec, M., S. Kralj, Z. Bradač, and S. Žumer. "Annihilation of nematic point defects: pre-collision and post-collision evolution." The European Physical Journal E 20, no. 1 (2006): 71-79.

Virga, E.G., 2018. Variational theories for liquid crystals. Chapman and Hall/CRC.

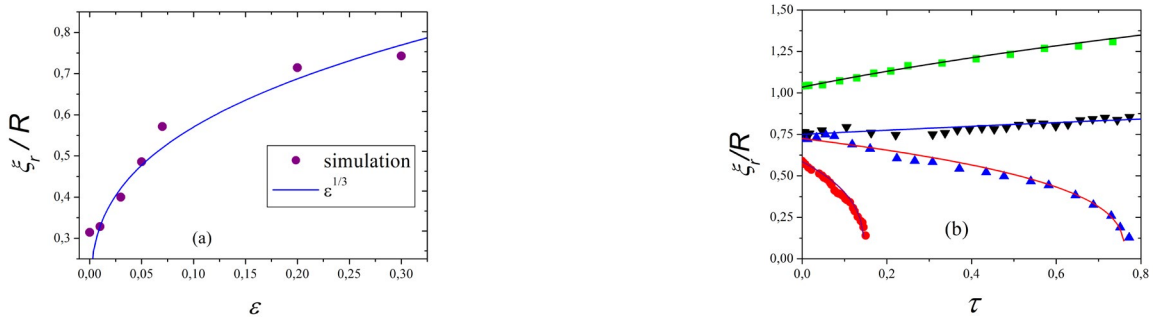

Fig. 5. (a) $\mu_0(\varepsilon)$ representation at the $\tau = 0$ with dots, compared with the $\varepsilon^{1/3}$ ansatz. (b) Time evolution of the loop structure size for various ε: circles (ε=0.02), up triangles (ε=0.05), down triangles (ε=0.07), and squares (ε=0.2). The solid lines result from the model described by the equation (13).